Chapter 3 -Basic Acoustic Modeling

3.1-The Process

In the proposed process for modeling thermoacoustic instabilities the acoustics of the combustion chamber plays an important role in determining the system's stability. During the summer of 1999, experimental acoustic testing of cold, no flow conditions was conducted on the test rig shown in Chapter 1. The objective was to determine a system frequency response function relating a random noise speaker input and microphone outputs at various locations. This experimental data was used to validate analytical models that predicted identical frequency domain information for the test rig.

Figure 3.1 shows a schematic of the single injector test rig. The rig is a fairly simple system consisting mostly of a multiple number of varying diameter tubes. However, there are a few components in the test rig that present modeling difficulties. The most difficult section is near the combustion liner. As the drawing shows, there are three different paths that air can take to go from the inlet air plenum to the exit of the liner. Therefore, boundary conditions are needed at the injector inlet plane and the liner exit in order to accurately predict the acoustics of this section. To complicate matters even more, these parallel paths are not isolated from each other. Certain liners have perforated walls, allowing the pressure field from inside the liner to communicate with the pressure field outside the liner. Thus, some impedance must be found to account for how the perforates affect the acoustic pressure and velocity fields.

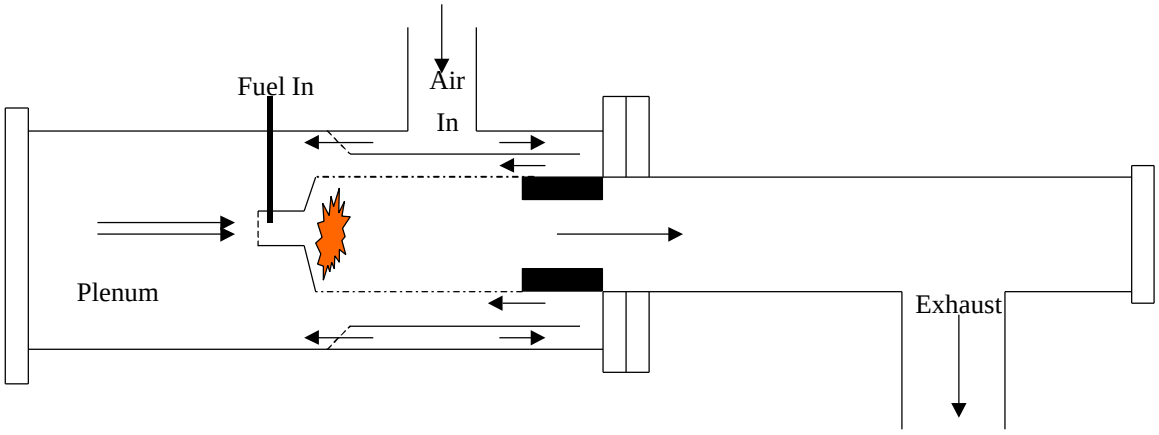

Figure 3.1-Schematic of single injector test rig.

Even though the acoustics are relatively simple, the model must be very accurate in order to make stability predictions for the overall system. It is critical that each section is properly modeled and coupled together. In the initial stages of modeling it was realized that an entire system model for an enclosure of such complexity would probably not match the experimental data. In addition, modeling the entire system would make it difficult to identify which sections were not modeled properly. Therefore, in order to understand each component and the coupling of components, models were created for many of the test rig sub-systems. With simple sub-systems, experimental tests could be conducted to verify the analytical models. There are many advantages associated with modeling each sub-system before the entire system. Simple sub-systems allow for easy assembly and retrofitting to obtain specific information which could never be isolated in the entire system. If the modeling technique does not work for a specific section, then the problem can be corrected at this lower level before moving on to the next level of complexity. This makes it much easier to isolate problems in the modeling process.

In order to create an analytical acoustic model, the 1-D wave equation (Equation 3.1a) is solved with the appropriate boundary conditions.

$$\frac{\partial^2 p}{\partial x^2} = \frac{1}{c^2}\frac{\partial^2 p}{\partial t^2} \quad (3.1a)$$

$$p(x,t) = Ae^{j(wt-kx)} + Be^{j(wt+kx)} \quad (3.1b)$$

The solution of the 1-D wave equation (Equation 3.1b) is a summation of 2 terms, with **A** being the complex amplitude of the forward traveling wave term, and **B** being the complex amplitude of the reverse traveling wave term. These amplitude constants must be determined by the boundary conditions of the system. The approach used for modeling one-dimensional acoustics is known as a 1-D transmission line technique. Each section of the system must have 2 boundary conditions since there are 2 unknown amplitudes which must be determined in order to describe the acoustic waves in each particular section. Once the boundary conditions have been determined, there will be 2N simultaneous equations to solve for the pressure field in N sections of the system. In matrix notation the equations would look like **Ax=b**, where **A** is a 2Nx2N matrix, **x** is a

2Nx1 vector containing the unknown constants, and **b** is a 2Nx1 vector containing any forcing which is applied at the boundaries. To solve for **x**, the matrix **A** must be inverted to obtain $\mathbf{x}=\mathbf{A}^{-1}\mathbf{b}$.

There are many acoustic boundaries in practical systems which do not have mathematically simple boundary conditions. If simple boundary conditions do not exist then an impedance for the boundary must be found either experimentally or from some empirical correlation. Specific acoustic impedance (Z) is defined as **p/u**, where **p** is the complex pressure, and **u** is the complex particle velocity. Equation 3.2, known as Euler's equation, provides a relationship between pressure and particle velocity.

$$r\frac{\partial u}{\partial t}=-\frac{\partial p}{dx} \quad (3.2)$$

This equation is derived from a force balance on a small element of fluid which is assumed inviscid. Euler's equation provides a relationship between pressure and particle velocity so that the boundary conditions which contain velocity terms can be written in terms of the unknown pressure coefficients.

The boundary conditions can be determined by using conservation laws. At boundaries which do not have sources or losses, conservation of acoustic volume velocity and pressure must be maintained. At source boundaries either the velocity or pressure of the source is matched with the velocity or pressure produced by the source. Figure 3.2 shows diagrams of two different simple boundary conditions. At a rigid wall, the boundary clearly has zero velocity ($u_{wall}=0$), therefore the acoustic particle velocity at the wall must also be zero ($u_{part}=0$). At a boundary where the area changes $u_1S_1=u_2S_2$, and $p_1=p_2$.

Figure 3.2-Rigid wall and area change boundaries.

The first condition comes from a control volume approach where the mass into the control volume must equal the mass leaving the control volume. The assumptions made here are that there are no sources or sinks, and that the gas is incompressible. The second condition is derived from a force balance on a control volume.

From the modeling process outlined above, it is desired that a detailed understanding of each sub-system can be obtained before the entire system is assembled. The 1-D transmission line technique simplifies the actual acoustic field which makes the modeling easier, but at the same time some of the model's resolution is lost. Simply stated, information about the other two dimensions is lost in a 1-D approach. Since the dynamics of interest are at low frequency (0-800 Hz), and the L/D ratios are generally large, a 1-D model should capture most of the important lower order longitudinal modes. To capture the entire acoustic field, higher order radial (Bessel) modes must be included. These modes are important in the "near field" of a boundary, but their effect is dissipated as the acoustic wave moves away from the local area of the boundary. It is well known that the radial evanescent modes dissipate very quickly (See Pierce [24]), so in long sections where there are no boundaries these modes have no affect on the analytical model. It is not clear though, how the acoustic "near fields" affect each other, if for instance, there is a sudden area restriction and expansion near each other. Because of their relative closeness, the near field of the restriction may not dissipate before the near field of the expansion becomes important. By modeling smaller sub-systems these kinds of potential problems can be isolated in an experiment to test the validity of a 1-D model.

Another important reason for modeling sub-system's is to see if the models are accurate enough to allow for the use of linear system theory to determine the frequencies at which instabilities can occur. For successful stability predictions the phase must also be known very precisely because an instability frequency will occur only at frequencies where the system phase passes through either 0° or 180°, providing the corresponding gain is greater than unity at the crossover frequency. If the phase is not correct, then there can be a larger degree of uncertainty in determining at exactly which frequency the instability will occur. In the remainder of this chapter, sub-system models will be created and analyzed to show if the 1-D approach is accurate enough to allow for the precise

determination of instability frequencies in enclosure geometries similar to those found in the Solar Turbine test rig.

3.2-Speaker Modeling

In order to excite the acoustics of a system, some form of acoustic source is needed. A speaker placed in the system acts as a velocity source to drive the system. The speaker model consists of two parts, one being the dynamics of the electrical circuit, and the other being the mechanical dynamics of the speaker cone. The entire acoustic system model has a transfer function relating the system output (velocity or pressure) to the system input (voltage supplied to the speaker). The boundary condition at the speaker cone matches the speaker cone velocity with the velocity of the air next to the speaker. Therefore, a transfer function must be created between the input voltage and the speaker cone velocity.

Figure 3.3 shows diagrams of both the standard electrical circuit and the mechanical mass-spring-damper used to model both the electrical and mechanical parts of the speaker.

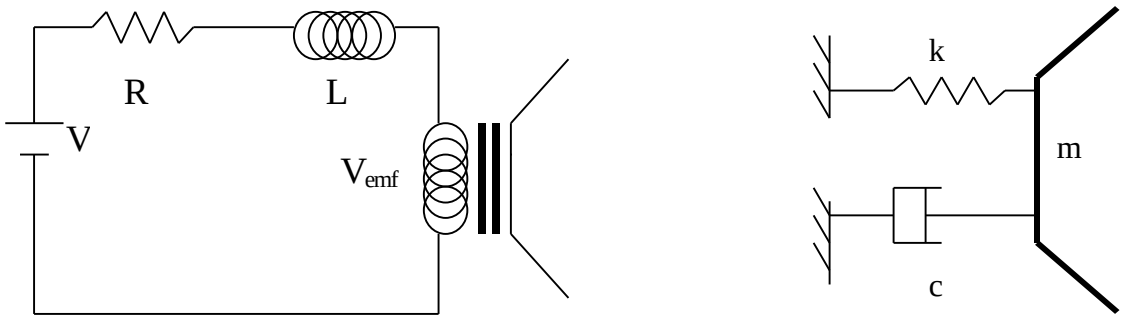

Figure 3.3-Speaker electrical and mechanical models.

Using Kirkoff's voltage law, $\Sigma V_{loop}=0$, one obtains Equation 3.3. Because all of the components in the system are dynamically changing it is assumed that all quantities such as voltage, current, velocity, and forcing are harmonic, so that they will all have solutions of the form $Ae^{j\omega t}$ where A is the magnitude constant. By differentiating the inductance term the equation can be written as a function of the current variable. Equation 3.4 is the mechanical model derived from Newton's second law, $\sum F_{ext}=ma$. The forces on the

speaker include damping (c dx/dt), stiffness (kx), and the electrical input force (Bli) which generates the back EMF. By differentiating and integrating the position and acceleration terms, respectively, all of these terms can written as a function of the velocity variable. The electrical current term in Equation 3.4 can be replaced with Equation 3.3, which was solved in terms of the current, to obtain Equation 3.5. This equation is a transfer function between the input voltage (V_{in}) and the speaker output velocity (dx/dt).

$$\sum V_{loop} = V_{in} - iR - jwiL - Bl\dot{x} = 0 \quad (3.3)$$

$$\sum F_{ext} = m\ddot{x} = -c\dot{x} - kx + Bli \quad (3.4)$$

$$\frac{\dot{x}}{V_{in}} = \frac{Bl}{(R + jwL)(mjw + c + \frac{k}{jw}) + (Bl)^2} \quad (3.5)$$

Once the analytical model has been made the constants in the model must be determined experimentally. The goal is to find values for the constants and then compare the speaker model to an experimental test to fine tune the values. Equation 3.4 can be written in a standard form by dividing each term of the equation by the mass which yields Equation 3.6 where $2\xi\omega_n$=c/m and ω_n^2=k/m. ξ is defined as the damping ratio and ω_n is the natural frequency.

$$\ddot{x} + 2xw_n\dot{x} + w_n^2 x = Bli \quad (3.6)$$

The mechanical constants (m and k) are determined from the speaker's natural frequency. At the speaker's natural frequency the response to a given voltage input is a maximum. Therefore, in Equation 3.3 the back EMF term is also a maximum at resonance since it is a function of the speaker's velocity. If a small test resistor is placed in series with the speaker, then the voltage drop across the resistor can be measured while sweeping through the frequency spectrum. Because the back EMF is a maximum at resonance the voltage drop across the test resistor will be a minimum. Two independent natural

frequency values are needed since there are two constants, the mass (m) and stiffness (k), which must be determined from the natural frequency. One can be determined using the small test resistor technique explained above. To obtain a modified natural frequency value, a small mass is added to the speaker cone. The new mass loaded natural frequency is then found from $\omega_n=\sqrt{k/(m+m_{known})}$. With two unknowns and two equations the unknown constants k and m can be found. The mechanical damping (c) is very difficult to measure so its value is assumed and then adjusted during the comparison between the analytical model and the experimental data.

Determining the electrical speaker constants is very straightforward. The resistance (R) is obtained with a multi-meter, and the inductance (L) can be found with an inductance meter. The magnetic field constant (B), and the length (l) of the coil are found together (Bl) from the static form of Equation 3.4. If all the dynamic terms of Equation 3.4 are neglected, then the only terms left are the static displacement (kx) and the static input force (Bli), where the current is assumed to be a DC quantity. The stiffness (k) is known from the natural frequency test. If a constant current is applied to the speaker, then the speaker will respond with a constant displacement (x). The current can be measured with a multi-meter, and the displacement can be measured with a feeler gauge, allowing for an approximate determination of the Bl constant.

Because of experimental variation between 30-40%, and the fact that some of the constants must be found using simplified analytical equations, there is a need to "fine-tune" the model's values. The best technique is to compare the analytical model with an experiment. This shows how accurately the analytical model represents reality. Initially, the plan was to model a system which consisted of a speaker on the end of a PVC pipe. After performing experiments and generating an acoustic model it was found that the model did not match with the experiment data. Because the speaker was coupled with the tube acoustics it became very difficult to determine which part of the coupled system was not modeled correctly.

In order to de-couple the system the speaker was modeled as a baffled piston radiating into the open air. The piston is broken into small differential mono-pole sources. These sources can be integrated over the piston surface to obtain the pressure field as a function of the distance away from the mono-pole sources as shown in Equation

3. 7. Equation 3.7 relates the speaker cone velocity (U_0) to pressure. The velocity can be related to the voltage through the speaker model which then provides an input/output relationship between voltage and pressure. To obtain experimental data of this system a speaker was driven with white noise from 0-1600 Hz while radiating into the open air. A microphone was placed approximately ¼" from the speaker cone face in order to capture the pressure field emitted from the speaker.

$$P(r,0,t) = rcU_0\{1-e^{-jk(\sqrt{r^2+a^2}-r)}\}e^{j(wt-kr)} \quad (3.7)$$

Using the dynamic equations presented so far, the experimentally determined constants were inserted into the model and compared with the experimental data. Magnitude and phase plots of the frequency response function (FRF) plotted in Figure 3.4, shows poor matching between the experiment and model. There are six constants (Bl, m, c, k, R, L) which must be fine-tuned, therefore some systematic way of determining these values is needed. The most critical speaker parameter to match is its first resonant natural frequency. Because most of the speakers used have highly damped resonances, the exact frequency of resonance must be determined from where the phase passes through 90°. Based on Equation 3.6, the natural frequency of a second order m-c-k system is the square-root of the stiffness divided by mass. By adjusting the stiffness to mass ratio the phase of the model can be made to cross 90° at the same frequency as the experiment. The mass and stiffness also affect the magnitude of the FRF above and below the resonant frequency. Equation 3.5 shows that the low frequency range is controlled by the k/jω term, while at higher frequencies the mjω term begins to dominate the response magnitude. Therefore, by adjusting the mass and the stiffness to match the resonant frequency while also controlling the low and high frequency magnitudes these two parameters can be fixed. It should be noted that these parameters needed only a 10-20% adjustment from the experimentally determined values for the speaker response shown in Figure 3.4. These adjustments are within the variation of 30-40% seen in the experimental data.

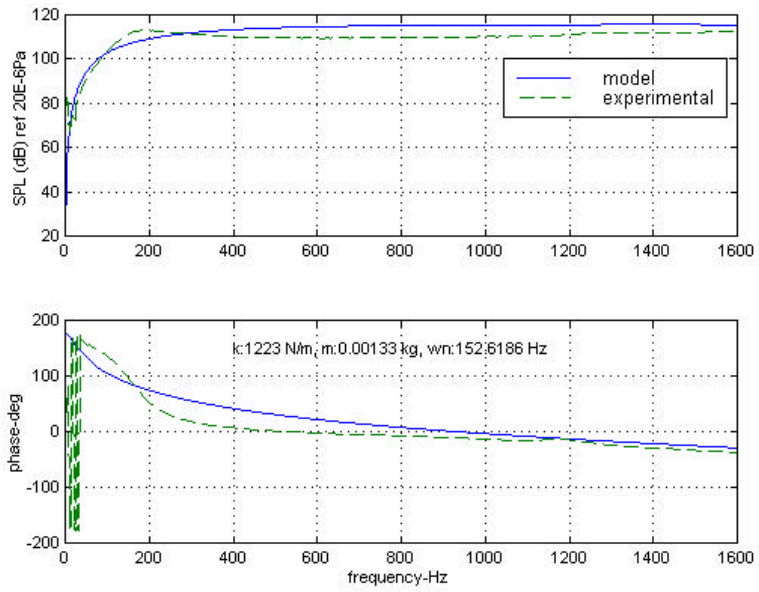

Figure 3.4- 3" Speaker FRF with experimentally determined constants.

Mass and stiffness values fix the resonant frequency, but the damping of the speakers resonance must still be corrected. Adjusting the damping not only changes the shape of the magnitude response, but also the slope of the phase as it changes through the resonant bandwidth. The roots in the denominator of the $(\dot{x}/dt)/V_{in}$ speaker transfer function (Equation 3.5) are the poles of the system. The exact values of these poles are found by solving a cubic equation, but knowing that the constant Bl term is very small in magnitude allows one to neglect the Bl term. If this is done, then the resulting cubic polynomial can easily be factored. Two of the poles are complex conjugates which come from the mechanical part of the speaker, and the third is a real pole found from the speaker's electrical circuit. Neglecting Bl does not affect the pole locations (resonant frequencies), but it does drastically affect the damping of each of these modes. The Bl constant is an electro-mechanical coupling term which adds damping to the system since Bl(dx/dt) represents the energy loss caused by the back EMF.

Figure 3.5 shows just how drastically Bl can affect the damping of the magnitude and the phase of the speaker FRF. The plots in Figure 3.5 show each pole plotted individually and then a composite FRF. Figure 3.5a shows the real electric pole, which has a high frequency resonance, so it does not affect the composite FRF near the speaker

resonance. It also shows the complex conjugate mechanical poles. These plots do not take into account the Bl term, but when the Bl term is added to the composite FRF the magnitude and phase becomes much more damped. Even though the damping of the composite plot increases, the resonant frequency does not change, as indicated by where the phase crosses 90°. In both the purely mechanical FRF and the composite FRF, the phase goes through 90° at the exact same frequency. Figure 3.5b shows the same electrical and mechanical FRF's, but the Bl term in the composite plot has been reduced in half. The composite plot approaches the purely mechanical FRF because of the reduction in damping at the speaker's resonance. Figure 3.5c is the same as the previous two plots except that the Bl term has been doubled in value. As expected, the speaker resonance becomes very highly damped.

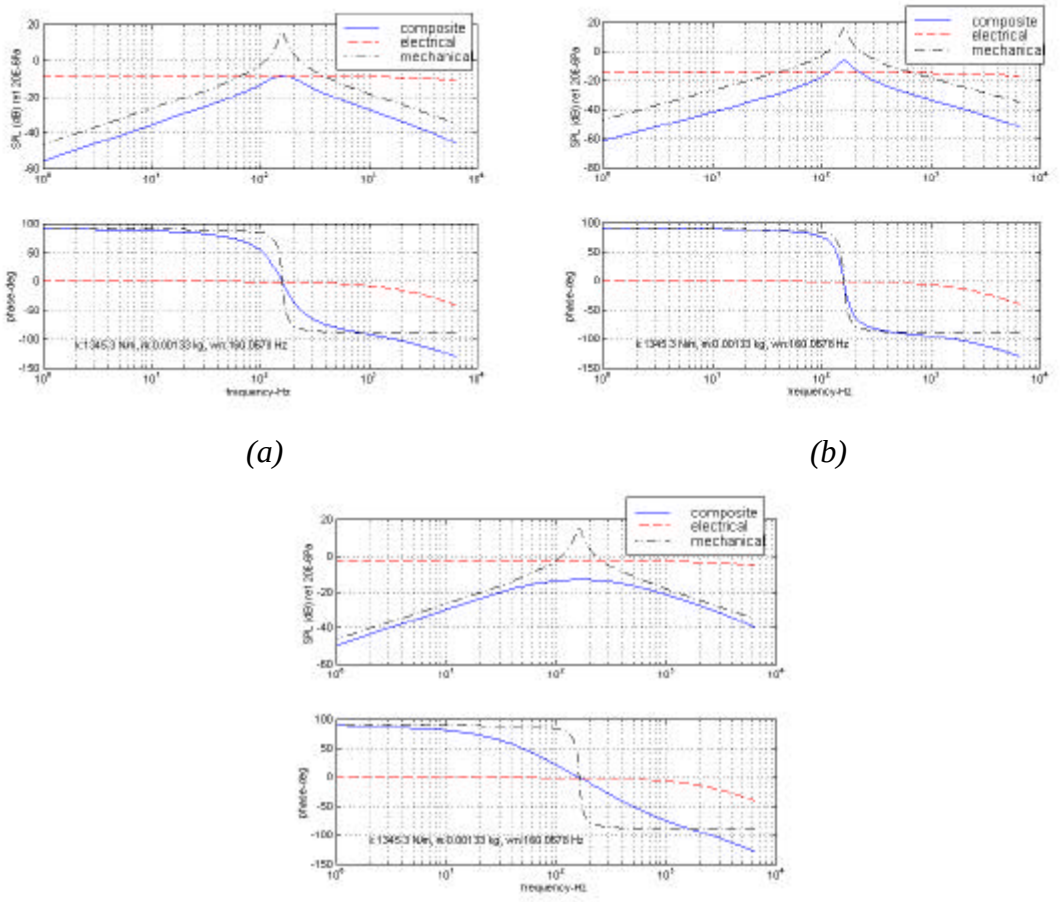

(a) *(b)*

(c)

Figure 3.5-Effect of Bl term on a speakers frequency response.

Based on the previous discussion, the Bl term can be adjusted to obtain the proper amount of speaker damping. The mechanical damping (c) is another term which adds damping to the system. This term is very hard to determine experimentally, therefore the amount of mechanical damping was assumed, and then adjusted to fine-tune the speaker's damping. Of the two forms of damping, the electrical-mechanical coupling term has a much larger impact on the damping of the speaker resonance.

The last two constants which have yet to be investigated are the purely electrical components R and L. As shown in Figure 3.5, the electrical resonance occurs over one decade higher than the speaker resonance. Therefore, its dynamics have very little effect on the low frequency response of the speaker (0-800 Hz). This pole (-R/L) can correct the model's higher frequency phase because the phase of the electrical pole begins to impact the phase of the composite system approximately a decade before the actual electrical resonance occurs. The adjusted parameter values produced a speaker FRF model which matched closely with the experimental data, as shown in Figure 3.6.

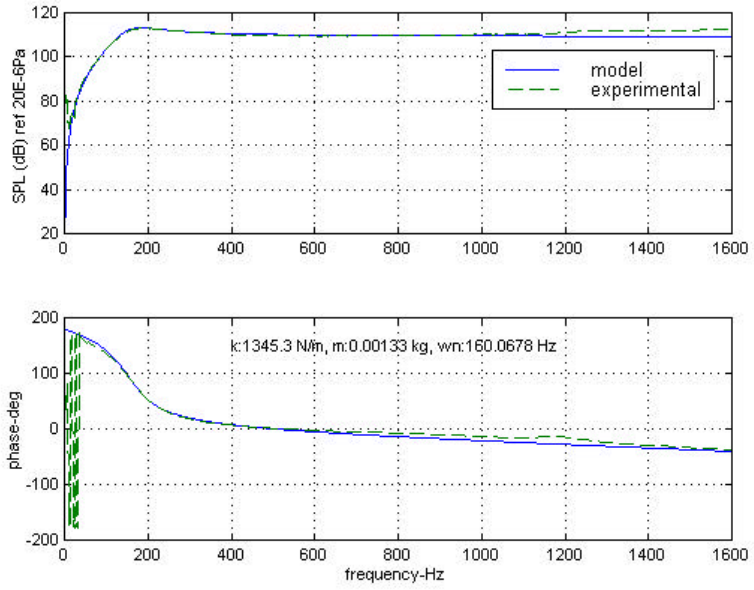

Figure 3.6-3" Speaker FRF with refined constants.

3.3-Tube Modeling

A few important geometries must be modeled in order to capture the dynamics of the most important parts of the test rig. As mentioned earlier, most of the test rig is composed of various diameter pipes, therefore the initial task is to make sure that a simple driven-pipe system can be modeled. Other important geometries include large area constrictions and expansions. Taking pressure field measurements close to the area changes will show how far the 'near field' propagates away from the boundary. All of the rig testing was done using a speaker to drive the system at approximately the same location as the flame. A tube model was also created to model a system which was not forced at a boundary and also not forced over an entire cross sectional area. This generates a parallel flow path at the speaker plane. The last important geometry to model was a perforated liner. After modeling all of these sub-system components the composite test rig model will be much easier to model and troubleshoot.

3.3.1-Closed-Driven Tube

A closed-driven tube is the simplest system to couple both tube acoustics and speaker dynamics. To generate an experimental model of this system a speaker was connected to the end of a PVC pipe as shown in Figure 3.7.

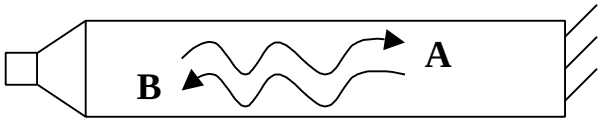

Figure 3.7- Diagram of the closed-driven system.

Initial attempts to model this simple system with high fidelity failed due to the lack of attention paid to details in the experimental setup. The first experimental model consisted of threaded PVC end-pieces that slid over the end of the pipe and then accepted a threaded PVC cap. The threaded end-pieces changed not only the tube diameter, but also the threads created a region of constantly changing area. It was thought that these slight area changes on each end would not affect the modeling process, but there were large discrepancies between the model and experimental data. Figure 3.8 shows an FRF

comparing the model to experimental data. In Figure 3.8 the model shows fairly good prediction of resonant frequencies, but the amplitude of each peak is off by 6-8 dB. The text in the plot provides information about the geometry of a particular test, and data about the speaker including its natural frequency. Parameters were adjusted to account for possible dissipative losses from the tube, and an incorrect speaker model, but the response changed very little. It was then realized that the small area changes from the threads might be generating changes in the experiment which were not being captured by the model. In order to eliminate all possible area changes in the model, the end pieces were removed and replaced by ¼" pieces of plexiglas so that a perfectly rigid boundary could be obtained. On the speaker end, a hole was cut in the plexiglas so that the speaker could be mounted.

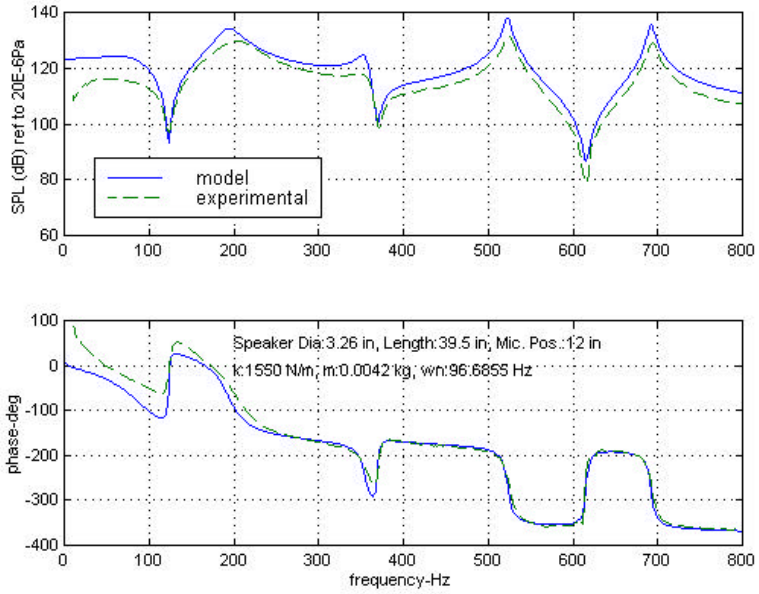

Figure 3.8-Comparison of experimental data and model of closed-driven tube.

The new experimental data was compared with the analytical model. As mentioned earlier, generating a transmission line model consists of matching volume velocities and pressures at boundaries. Only two boundary conditions exist in the simple closed-driven tube. Since the closed end of the tube is rigid, the air at that boundary must also be stationary, thus $u_1(x=L)=0$. At the driven end of the tube, the velocity of the air particles must match the speaker cone velocity ($u_1(x=0)=u_s=\Sigma F_{speak}/Z_{mech\text{-}speak}$). Equation 3.8 shows the matrix notation used to solve for the complex pressure amplitudes, **A** and

B, for the forward and reverse traveling waves. By inverting the matrix the pressure amplitudes can be obtained and then used in Equation 3.1 to find the P(x) for each frequency in the bandwidth of interest.

$$\begin{bmatrix} e^{-jkL} & -e^{jkL} \\ (S_s + \frac{Z_m}{rc}) & (S_s - \frac{Z_m}{rc}) \end{bmatrix} \begin{bmatrix} A \\ B \end{bmatrix} = \begin{bmatrix} 0 \\ \frac{Bl}{R + Ljw} \end{bmatrix} V_{in} \quad (3.8)$$

Because the speaker is at a boundary, the forces applied to the speaker include more than just the electrical driving force. At the boundary, there is a pressure differential between the ambient pressure on the outside and the acoustic pressure on the inside. The pressure differential generates a force which couples the tube acoustics and the speaker. If the speaker and the tube are uncoupled they can be thought of as independent systems each having their own dynamics, but with the pressure coupling the systems are not independent and their dynamics are determined by the coupled system. This can be seen in Figure 3.9 where the reactive part of the mechanical impedance (Im{Z}) is plotted for both the speaker and the tube. In the uncoupled problem, resonance would occur when the reactance of each individual system equaled zero. In the coupled system resonance occurs when $\mathrm{Im}\{Z_{m\text{-}speak}+Z_{m\text{-}tube}\}=0$; therefore the condition which must be satisfied for resonance is that $\mathrm{Im}\{Z_{m\text{-}speak}\}= \mathrm{Im}\{Z_{m\text{-}tube}\}$. In Figure 3.9 the resonance condition is met when the impedance lines for each sub-system cross. The first crossing of the speaker and tube reactance occurs very close to where each sub-system crosses zero, but subsequent crossings deviate substantially from where the tube would normally have zero reactance, thus changing where one would normally expect resonance to occur for a closed-closed tube.

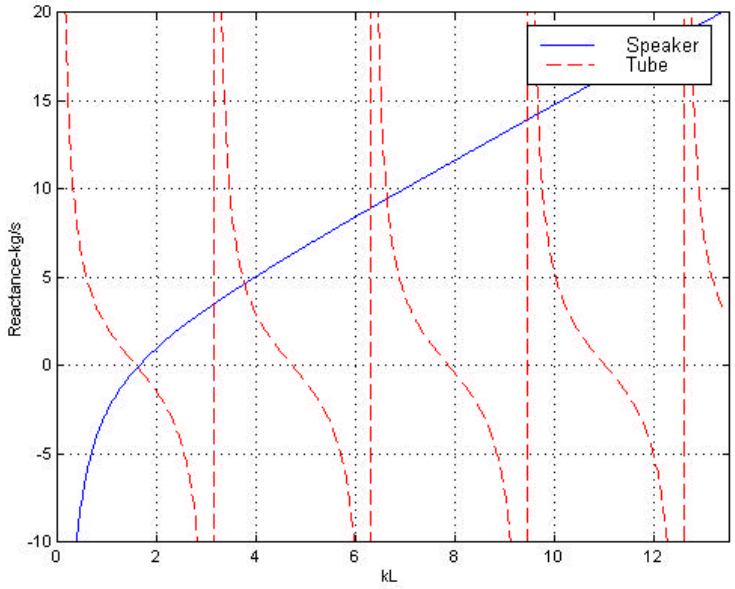

Figure 3.9-Reactive part of speaker and tube impedance.

Once the complex pressure amplitudes were calcualated as a function of the input voltage (V_{in}), the transfer function (p/V_{in}) was generated and compared with the experimental tube data as shown in Figure 3.10. The model predicts all the resonances within ~1 Hz with a maximum magnitude deviation of 2 dB and a maximum phase deviation of 15°. The microphone output was taken 10" away from the speaker in a 35.75" long pipe, but microphone responses taken in other locations produced similar results. The differences in the low frequency band (0-75 Hz) are most likely due to the lack of a bulk mode in the model. This bulk mode would be generated if the system had openings where air could escape, which is certainly possible around the speaker. Attempts to model these small air gaps are very difficult since the geometry and size of the gaps are unknown. Theoretical impedance values for holes with specific geometries will be used later to model perforated plates.

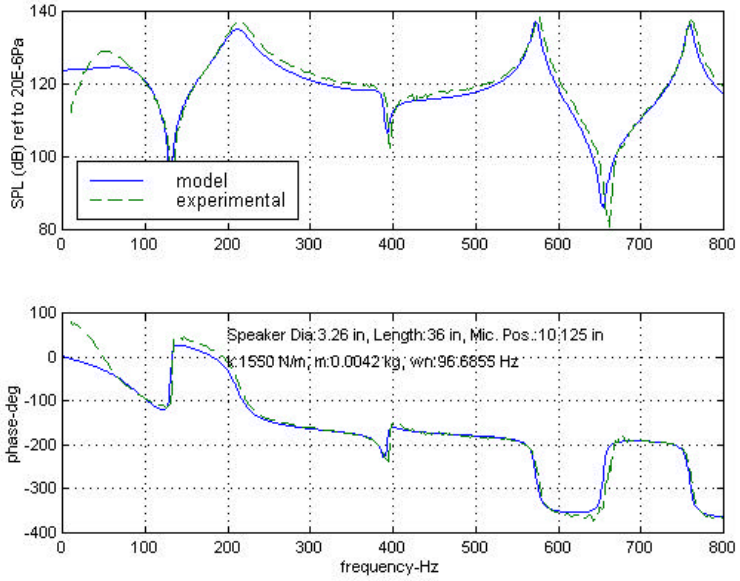

Figure 3.10-FRF comparison of experiment and revised model for closed-driven tube.

As stated earlier, the main purpose of the driven-pipe tube was to make sure that a simple tube could be modeled with a coupled driver. Based on the results in Figure 3.10 these goals were accomplished. As with the speaker, it is very important to know the values of all the fixed constants. Also important is making sure all the geometric components of the system are modeled. Any unmodeled geometries, such as the threaded end caps, cause changes in the acoustic response of the system which can not be accounted for if they are not modeled. With the knowledge gained from this simple tube model, more complex models can now be attempted.

3.3.2-Closed-Driven Tube with Area Restriction

A closed-driven tube with an area restriction is very similar to the closed-driven tube except for the fact that an area restriction and expansion is placed in the middle of the tube as shown in Figure 3.11. The purpose for modeling this geometry was to reproduce the large area reduction seen from the inlet air plenum to the injector, and also the area expansion from the injector to the combustion chamber. The area reduction ratio chosen was 16:1 which is comparable to the area changes seen in the test rig. Drastic area restrictions and expansions over a small injector length may result in a coupling of

the near fields inside the injector. If this were to occur the acoustic pressure field would not be accurately predicted using a 1-D model. In an attempt to determine if the 1-D model can predict the correct pressure field, it will be compared with experimental data.

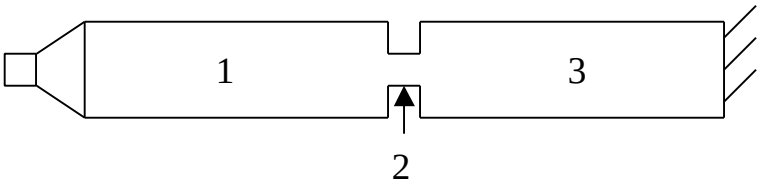

Figure 3.11- Diagram of closed-driven tube with area changes.

The analytical model for this system can be created by following the same conservation principles used in the previous models. The new boundary conditions in this model are continuous pressure across the area changes and also conservation of volume velocity. At each change in geometry new complex pressure amplitudes must be calculated. Therefore, for this system, 3 sets of complex amplitudes must be calculated using a 6x6 matrix. Figure 3.12a shows a FRF of this system with the microphone in section 1, ¼" away from the area restriction between sections 1 and 2. This FRF indicates that the near field decays quickly from the large area change, allowing the 1-D model to capture most of the relevant dynamics near the abrupt area change. Figure 3.12b is an FRF with the microphone 3" away from the rigid boundary in section 3. From both of these FRF's, two interesting observations can be made. First, the system acts as a low pass filter in the bandwidth considered ($kL<1$). In Figure 3.12b the resonant frequencies peak magnitude decreases with increasing frequency. This indicates that, as the frequency increases, the power transmission loss through the area constriction also increases, thus lowering the acoustic pressure.

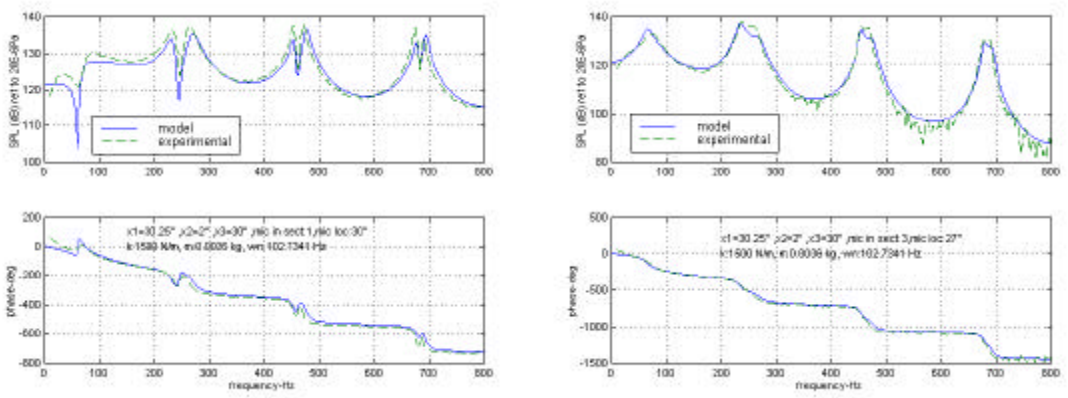

Figure 3.12-FRF comparison of experimental and model for closed-driven tube with an area restriction.

Secondly, each of the large sections act as very distinct sub-systems as indicated by the two closely spaced peaks in the FRF's. The first "sub-system" mode (f_1) occurs at 230 Hz with higher harmonics occurring at almost double the frequency of the previous "sub-system" harmonic ($f_N=Nf_1$,N=1,2,3…). The doubling in frequency of each successive harmonic indicates that half-waves are being formed in a length that corresponds to a 230 Hz frequency through the relationship $\lambda f=c$. The length associated with a 230 Hz half-wave is approximately 30", which corresponds to one of the sub-system's lengths. Section 3 most closely resembles a closed-closed pipe which promotes the formation of half waves, thus the peak at 230 Hz and its harmonics are caused by half-waves formed in the section 3. This also indicates that the other closely spaced peaks must be due to the sub-system of section 1. The fundamental and harmonic frequencies of this sub-system indicate that it does not behave like a closed-open tube, a closed-closed tube, or anything in-between. The speaker boundary acts to stiffen the sub-system causing a higher than expected fundamental resonant frequency. The major peak below 100 Hz is a system mode which occurs at a lower frequency than would be expected for a simple half-wave forming in the entire length of the pipe. The important conclusion is that the sub-system modes dominate the response of the system, therefore the acoustic frequencies are determined by the length of each sub-system because the area restriction acts like a hard boundary. This does not preclude the formation of a complete system mode, as indicated by the resonate peak at 70 Hz, but it does show that sub-system modes can dominate the system response.

In conjunction with the area restriction study, a parametric analysis was conducted on a closed-closed and closed-open pipe geometry with an area change as shown in Figure 3.13. The parameters varied were the lengths and areas of each section. This simple geometry allows for a closed-form solution of the eigenvalues, or natural frequencies, of the system. Applying the appropriate boundary conditions leads to a 4x4 coefficient matrix as shown in Equation 3.9 for the closed-open configuration. The system eigenvalues are found by taking the determinate of the matrix and equating it to zero. Equations 3.10a and 3.10b result from the evaluation of the determinate for the closed-closed and closed-open cases, respectively. The natural frequencies have been non-dimensionalized using kL where k is the wave number ω/c.

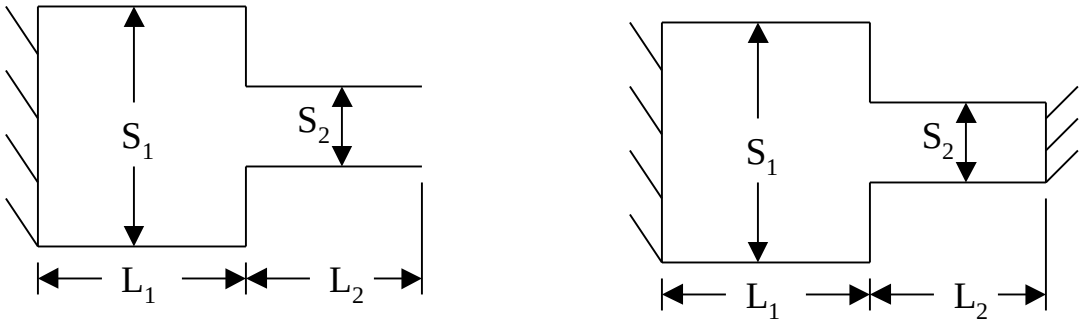

Figure 3.13-Schematic of closed-open and closed-closed geometries.

$$\begin{bmatrix} 1 & -1 & 0 & 0 \\ e^{-jkl_1} & e^{jkl_1} & -1 & -1 \\ S_1 e^{-jkl_1} & -S_1 e^{jkl_1} & -S_2 & S_2 \\ 0 & 0 & e^{-jkl_2} & e^{jkl_2} \end{bmatrix} \begin{bmatrix} A_1 \\ B_1 \\ A_2 \\ B_2 \end{bmatrix} = \begin{bmatrix} 0 \\ 0 \\ 0 \\ 0 \end{bmatrix} \quad (3.9)$$

$$\frac{S_2}{S_1} = -\cot\left(\frac{kL}{r+1}\right)\tan\left(\frac{kL}{1+\frac{1}{r}}\right) \quad (3.10a)$$

$$\frac{S_2}{S_1} = \tan\left(\frac{kL}{r+1}\right)\tan\left(\frac{kL}{1+\frac{1}{r}}\right) \quad (3.10b)$$

Figures 3.14a and 3.14b show how the natural frequency (kL) varies with the area ratio S_2/S_1, and also the length ratio $r=l_1/l_2$ for the closed-closed and closed-open cases. As the area ratios approach 1 in Figure 3.14a, kL approaches π, 2π, 3π… which corresponds to half waves $\lambda_1=2L$, $\lambda_2=L$, $\lambda_3=2L/3$…. This is expected for a closed-closed tube in which pressure must be a maximum at each boundary. For area and length ratios different from 1 the natural frequency can be either higher or lower than the assumed half-wave frequencies. In Figure 3.14b the exact same phenomena can be observed except that now when the area ratio approaches 1, kL approaches $\pi/2$, $3\pi/2$, $5\pi/2$…. This corresponds to quarter waves $\lambda_1=4L$, $\lambda_2=4L/3$, $\lambda_3=4L/5$… as expected for a closed-open configuration where pressure is a maximum at the closed boundary, and nearly zero at the open boundary. The analysis shows that area changes, and the relative lengths of each section, can greatly shift the acoustic resonant frequencies away from those expected based on the end boundary conditions only. Also, the extreme cases can be analyzed to see that, for example, in the closed-open case when S_2 becomes much greater than S_1, quarter waves form in section 1 since the area of section 2 is so large that it looks like an open boundary. Many other cases can be analyzed using the parametric plots of Figures 3.14a and 3.14b.

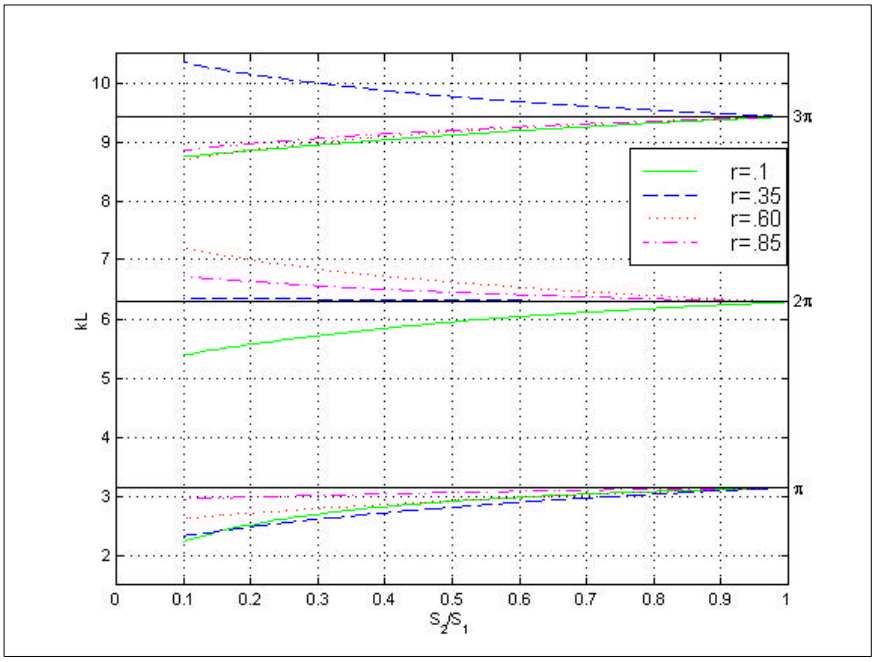

(a)

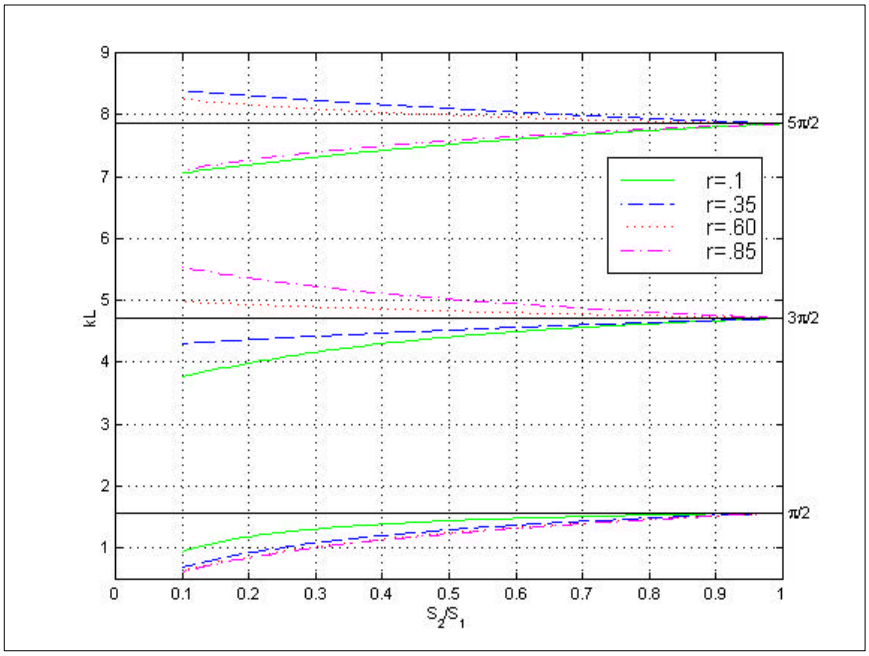

(b)

Figure 3.14a,b: (a)-First 3 modes of closed-closed tube with area and length variations. (b)-First 3 modes of closed-open tube with area and length variations.

3.3.3-Internally Driven Closed-Closed Tube

In the full scale rig, the acoustic testing was done using a speaker mounted internally near the injector inlet to the combustor where the flame likely resides. Also, the speaker was much smaller than the cross sectional area of the combustion liner. At the speaker plane, the acoustic pressure and velocity are not uniform across the entire plane making it very difficult to model this boundary in 1-D. Because of these potential complications it was crucial to learn whether the acoustics of this type of geometry could be captured using a 1-D model. Therefore, a 2" speaker was hung in a 4" diameter pipe with rigid boundaries on both ends to see if the model could capture this effect. Figure 3.15 shows the system arrangement.

Figure 3.15-Schematic of internally driven closed-closed tube

The initial approach was to model the speaker plane as a boundary where the volume velocity of the incident wave on each side of the speaker had to equal the speaker cone velocity, as determined by the speaker dynamics and the input voltage. Figure 3.16 shows the model's response compared to the experimental data. Obviously, this approach does not capture the actual pressure field at the speaker because there are two paths for the acoustic waves to take in the speaker plane. From the initial approach it was not clear whether the failure was caused by not including a parallel path, or if the general 1-D transmission line approach was unable to capture the dynamics of this system. In order to see if a 1-D approach could possibly work, a modal solution was attempted.

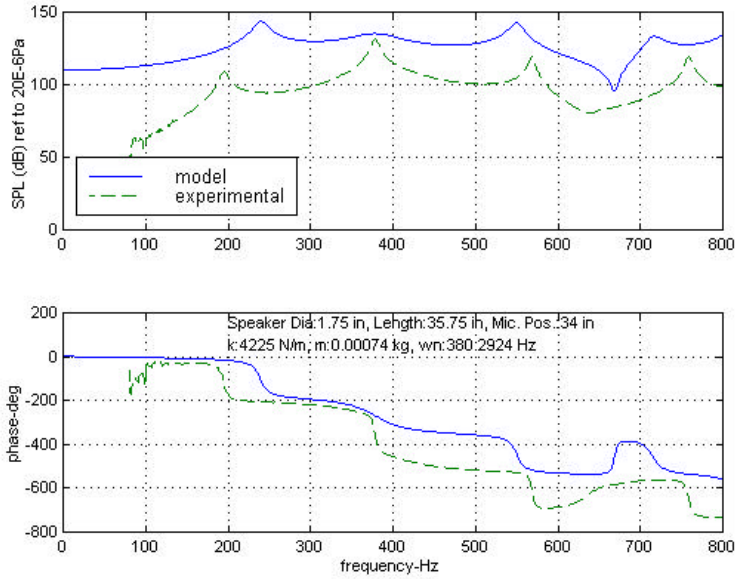

Figure 3.16-FRF comparison of model and experimental data for an internally driven closed-closed tube with acoustic velocity equaling speaker cone velocity at speaker boundary.

The modal solution involves solving the forced acoustic wave equation using separation of variables. Equation 3.11 shows the wave equation with two dirac delta forcing functions which model two monopoles out-of-phase. Two monopoles out-of-phase form a dipole, which is classically considered to be representative of a speaker's acoustic dynamics.

$$gP_0 \frac{\partial^2 p}{\partial x^2} - r_0 \frac{\partial^2 p}{\partial t^2} = -c^2 r_0^2 \frac{\partial u_s}{\partial t} A_s [d(x-(L_s+\frac{d}{2})) - d(x-(L_s-\frac{d}{2}))] = f(t) \quad (3.11)$$

$$\textbf{B.C.'s :} \frac{-1}{j\Omega r_0}\frac{\partial P(x=0)}{\partial x} = 0, \frac{-1}{j\Omega r_0}\frac{\partial P(x=L)}{\partial x} = 0$$

$$F_n(x) = A_n \cos(k_n x),\ k_n = \frac{mp}{L},\ m = n = 1,2,3... \quad (3.12)$$

The solution of Equation 3.11 is obtained by assuming that the equation is separable into functions of space and time (P(x,t)=F(x)Φ(t)). The spatial part is a second-order ODE with no damping, which is solved to provide the eigenvectors (mode shapes) and eigenvalues (natural frequencies) as shown in Equation 3.12. Once the eigenfunctions have been normalized, their amplitudes (A_n) can be found. The temporal ODE is found by assuming the solution is harmonic and applying Equation 3.12 to Equation 3.11. If both sides of the resulting equation are multiplied by F(x) and then each side is integrated over the volume to remove the spatial dependence, Equation 3.13 results. Since the integration over the volume of $F_n^2(x)$ was forced to equal 1 when the eigenfunctions were normalized, the spatial dependence can be eliminated from the left-hand side of Equation 3.11. On the right-hand side, integration of $F(x)\delta(x-x_0)$ results in the spatial function evaluated at x_0 ($F(x_0)$). By definition, the dirac delta function is equivalent to an impulse which is zero everywhere except where it is being evaluated. Therefore, integration over the entire length yields only the value of F(x) where the delta function is evaluated (x_0). Integration of the dirac delta functions in the other two dimensions (y,z) results in value of 1 for each dimension.

$$\ddot{\Phi}(t) + w_n^2 \Phi(t) = \sqrt{\frac{2}{V}} c^2 r_0 A_s \frac{du_s}{dt}\left[\cos(k_n(L_s+\frac{d}{2})) - \cos(k_n(L_s-\frac{d}{2}))\right] \quad (3.13)$$

$$u_s = \left(\frac{Bl}{R+Lj\Omega}\right)\frac{1}{Z_m} V_{in} e^{j\Omega t}$$

If both $\Phi(t)$ and the source velocity (u_s) are assumed harmonic, then the second-order ODE with forcing can be solved. When the time derivative of the source velocity is inserted into Equation 3.13, the input voltage (V_{in}) becomes the forcing term, and Equation 3.13 can be solved for the amplitude coefficients (B_n) of the temporal solution since it was assumed that $\Phi(t)=B_n e^{j\omega t}$. By combining F(x) and $\Phi(t)$ the pressure field is obtained as shown in Equation 3.14.

$$P(x,t) = F(x)\Phi(t) = \sum_{n=1}^{\infty} P_n(x,t) = \sum_{n=1}^{\infty} A_n \cos(\frac{np}{l}x) B_n e^{j\Omega t}, n = 1,2,3... \quad (3.14)$$

$$P_n(x,t) = \frac{1}{(w_n^2 - \Omega^2)} \frac{2}{V} c^2 r_0 A_s j\Omega \left(\frac{Bl}{R + Lj\Omega} \right) \frac{1}{Z_m} \left[\cos(k_n(L_s + \frac{d}{2})) - \cos(k_n(L_s - \frac{d}{2})) \right] V_{in} \cos(k_n x) e^{j\Omega t}$$

Equation 3.14 provides a relationship between the input voltage (V_{in}) and the output pressure (P), which can be used to create the FRF shown in Figure 3.17. Even though the pressure is a summation of an infinite number of modes, most of the information is contained in the first few modes, therefore only the first twenty modes were used to calculate the pressure. Also, the monopole separation distance (d) of ½" was determined by matching the model with experimental data. Physical insight can be gained by analyzing how the speaker interacts with the acoustic modes. Each mode has a characteristic mode shape, or eigenvector, excited by the speaker which can be thought of as a point force. If the point force location is near a node of a particular mode shape, then that shape will be excited very little. If, on the other hand, the point force is located near an anti-node, then that shape will be greatly amplified.

The model in Figure 3.17 shows very good agreement with the experimental data. An important feature of the configuration presently under investigation is that the speaker and acoustics are de-coupled. In the previous models, the speaker was "loaded" because of the ΔP across the speaker mounted at the boundary. With the speaker placed inside the tube, the pressure on both faces is the same, so the dynamics of the speaker become independent, or decoupled, from the acoustic dynamics of the system. This can be seen by looking at the system resonant frequencies. For a closed-closed tube 34" in length the half-wave frequencies are 187.5 Hz, 375 Hz, 562.5 Hz, etc…. The resonant peaks in

Figure 3.17 match very closely with the expected half-wave frequencies, which will only occur if the speaker's impedance is not modified by the tube's acoustic impedance. The speaker resonance (380 Hz) is highly damped and occurs very close to the full-wave frequency of the tube so it is difficult to see its magnitude, but the phase can be seen as a negative slope superimposed on the acoustic phase. The de-coupling of the driver from the system will make assembly of the system block diagram much easier because the speaker can simply be taken out of the system when the flame is inserted without affecting the dynamics of the acoustics.

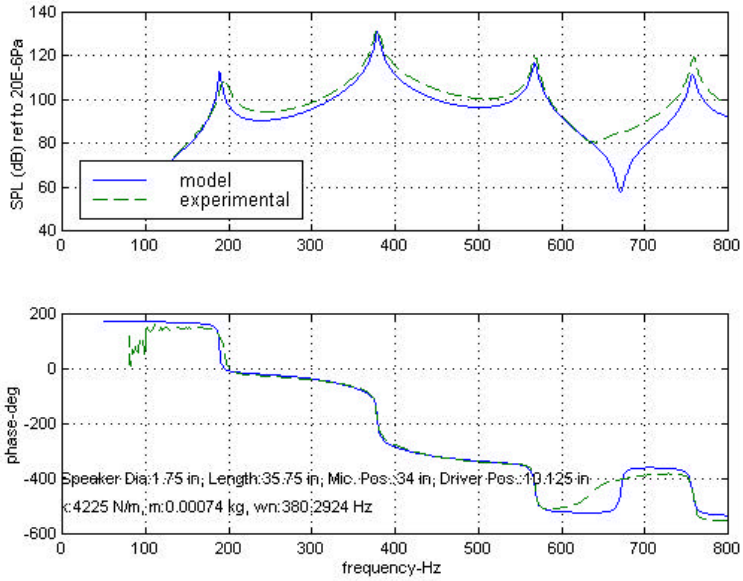

Figure 3.17-FRF comparison of modal model and experimental data for an internally driven closed-closed tube.

There is only one problem with the modal approach. Closed-form modal solutions exist only for very simple geometries such as closed-open or closed-closed tubes. Therefore, the modal model method will be useless for the single injector test rig which must ultimately be modeled. With this in mind, the 1-D transmission line approach was revisited. The initial modeling approach had failed because it could not capture the 2-D effects near the speaker. In an attempt to capture these effects the speaker plane was divided into parallel paths. One path would account for the speaker area, and the other path would account for the annulus area around the speaker. Figure 3.18a shows a schematic of the parallel path model with the appropriate boundary

conditions. The only new boundary condition is the volume velocity at the parallel path junction. At this junction, the total volume velocity entering the junction must equal the total volume velocity leaving the junction, seen in the velocity boundary conditions given in Figure 3.18a. The speaker itself is a dipole source of some finite thickness. The thickness is determined by matching the model's FRF to experimental data. Some thickness is necessary in order to maintain the continuous pressure boundary condition in the annulus around the speaker. If the speaker plane had no thickness, then the out-of-phase pressure waves from the dipole speaker would cancel each other out, producing no system forcing. Figure 3.18b shows the response of the 1-D transmission line model with parallel paths at the speaker plane. Allowing two paths at the speaker plane corrected the shortcomings of the initial transmission line model. The parallel path model also agrees very well with the modal model shown in Figure 3.17, proving that if a system is modeled correctly, the transmission line approach can handle certain 2-D effects. One phenomena that has yet to be explained is the occurrence of right half plane zeros in the experimental data taken when the microphone is located behind the speaker. Neither model predicts this unusual behavior and no plausible explanation exists for the right half plane zeros at this time. This problem only seems to occur for configurations where the speaker is hanging internally in a volume, as will be seen in future models. Right half plane zeros are ultimately important for control system performance, but do not greatly impact the models being developed here.

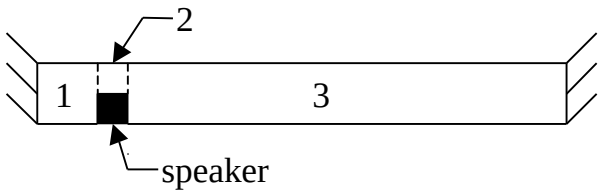

$V_1(x=0)=0$ $\quad$ $P_2(x=L_2)=P_3(x=0)$

$P_1(x=L_1)=P_2(x=0)$ $\quad$ $V_2(x=L_2)S_2+V_s(x=L_2)S_s=V_3(x=0)S_3$

$V_1(x=L_1)S_1=V_2(x=0)S_2+V_s(x=0)S_s$ $\quad$ $P_3(x=L_3)=0$

(a)

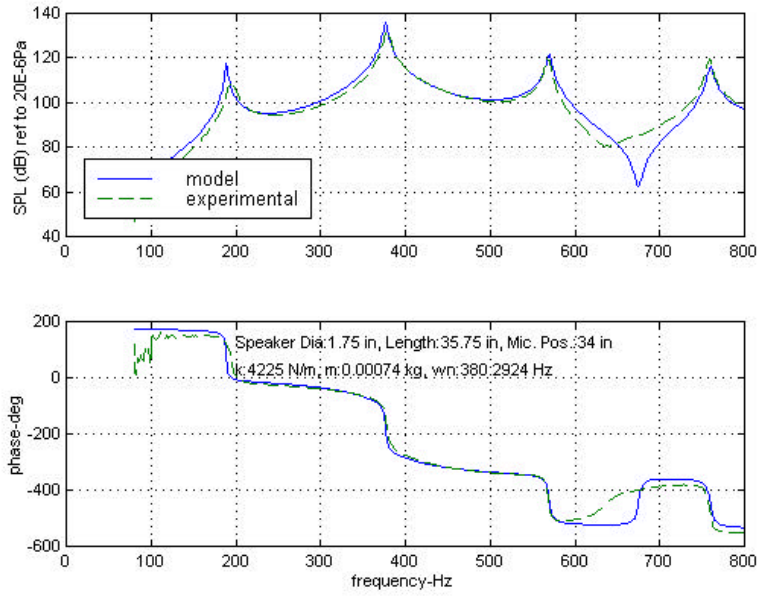

(b)

Figure 3.18a,b: (a)-Schematic of parallel path approach. (b)-FRF comparison of experimental data and transmission line parallel path approach.